

Scalp Diagnostic System With Label-Free Segmentation and Training-Free Image Translation

Youngmin Kim* Saejin Kim* Hoyeon Moon Youngjae Yu[†]
Yonsei University
{winston1214, 0110tpwls, mhy9910, yjy}@yonsei.ac.kr

Junhyug Noh[†]
Ewha Womans University
junhyug@ewha.ac.kr

Abstract

Scalp diseases and alopecia affect millions of people around the world, underscoring the urgent need for early diagnosis and management of the disease. However, the development of a comprehensive AI-based diagnosis system encompassing these conditions remains an underexplored domain due to the challenges associated with data imbalance and the costly nature of labeling. To address these issues, we propose “ScalpVision”, an AI-driven system for the holistic diagnosis of scalp diseases and alopecia.

In ScalpVision, effective hair segmentation is achieved using pseudo image-label pairs and an innovative prompting method in the absence of traditional hair masking labels. This approach is crucial for extracting key features such as hair thickness and count, which are then used to assess alopecia severity. Additionally, ScalpVision introduces DiffuseIT-M, a generative model adept at dataset augmentation while maintaining hair information, facilitating improved predictions of scalp disease severity. Our experimental results affirm ScalpVision’s efficiency in diagnosing a variety of scalp conditions and alopecia, showcasing its potential as a valuable tool in dermatological care.

1. Introduction

Approximately 80 million people in the United States are affected by male and female pattern hair loss [36]. Additionally, a study by Elewski *et al.* [14] reveals that nearly 90% of adults in the U.S. experience various scalp disorders. Among these, alopecia is especially common, impacting a significant portion of the population. The causes of alopecia are diverse, including aging, genetics, stress, and overall health conditions [46]. Therefore, early diagnosis is key to preventing the progression of these scalp-related diseases [35, 37].

*Equal contribution

[†]Co-corresponding author

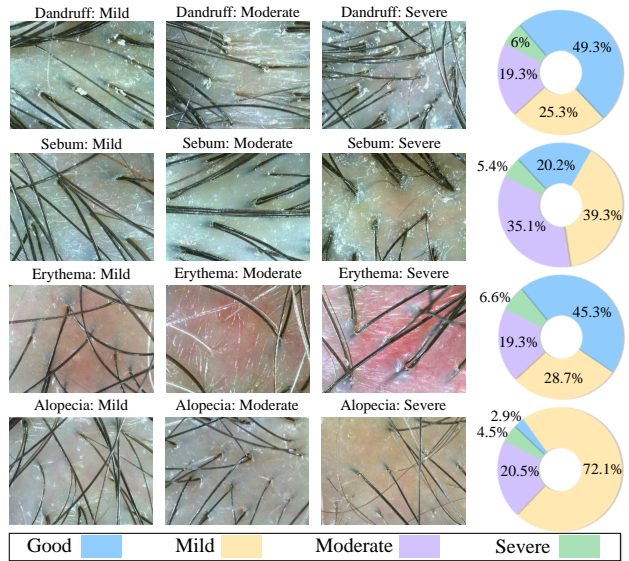


Figure 1. Data distribution and examples of AI-Hub microscopic scalp imaging training dataset. The images on the left side represent examples of each scalp disease condition at different severity and the charts on the right side represent data distribution of different severity within each scalp condition.

Recognizing the importance of early detection, numerous studies have explored scalp disease diagnosis using microscopic scalp imagery. For example, Chang *et al.* [7] proposed a scalp diagnostic system, Kim *et al.* [24] concentrated on follicle detection, and Seo *et al.* [43] identified features of hair loss for diagnosing alopecia. However, these studies often treat scalp and hair issues separately, overlooking a more integrated diagnostic approach.

Acquiring comprehensive labels for medical diagnostic systems presents a significant challenge in medical research. This difficulty primarily arises from the need for specialized domain knowledge in image annotation, which significantly increases labeling costs. Furthermore, data imbalance is a frequent issue, largely due to biases in

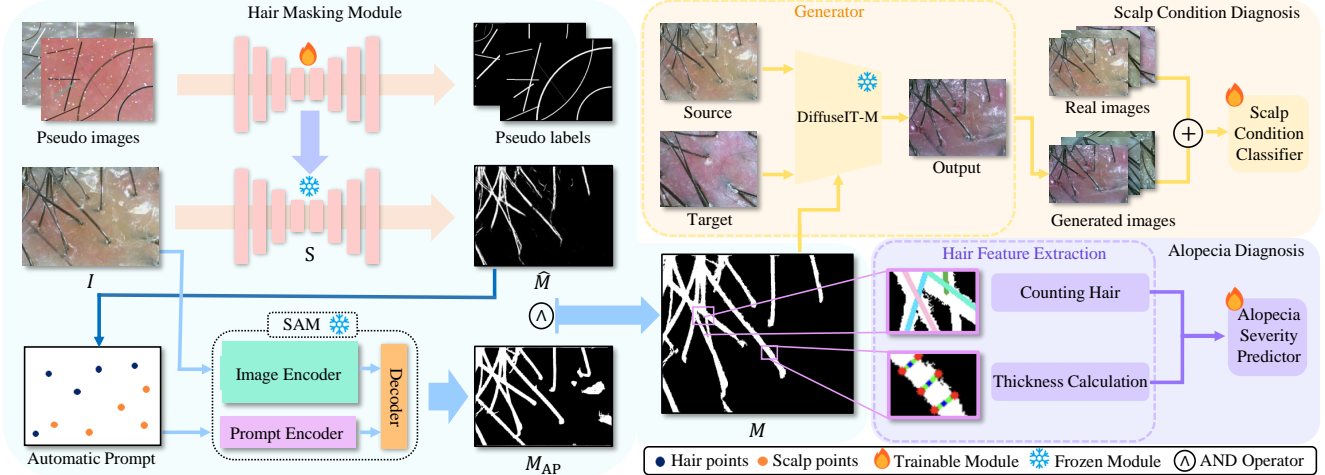


Figure 2. ScalpVision pipeline overview. Here, I denotes the original image. The hair segmentation mask generated by the segmentation model S , which is trained using a pseudo-training set, is represented as \hat{M} . The mask produced by the SAM is denoted as M_{AP} , and M signifies the final, combined hair segmentation mask. The “Automatic Prompt”, used for refining segmentation, is derived from \hat{M} .

the training process. For instance, most datasets focusing on scalp conditions disproportionately represent *healthy* scalps, leading to a scarcity of data on severe scalp diseases and alopecia. As a result, there are no publicly accessible datasets that offer detailed labels for both scalp conditions and alopecia in scalp images.

Despite the lack of publicly available datasets, we accessed a specialized dataset from AI-hub [1] for classifying the severity of scalp conditions and alopecia¹. This dataset categorizes the severity of scalp conditions, including dandruff, excess sebum, and erythema, into four levels (good, mild, moderate, severe) across 96K images. It also includes about 24K images for alopecia severity classification. The distribution of this dataset’s attributes is illustrated in Figure 1. However, this dataset lacks detailed information on hair and follicles, which is crucial for more in-depth diagnostic analyses.

To address these challenges, we developed “ScalpVision,” a comprehensive system designed for in-depth assessment of scalp health, as illustrated in Figure 2. ScalpVision’s pipeline integrates three key components: 1) hair segmentation, 2) diagnosis of scalp conditions, and 3) prediction of alopecia severity. The backbone of ScalpVision is its advanced segmentation technique. This technique employs label-free learning and zero-shot segmentation to effectively discern and extract hair-related features. It combines masks generated by a model trained on synthetic image-label pairs with those from the point-guided Segment Anything Model (SAM) [26]. For diagnosing scalp conditions, we leverage DiffuseIT-M, a diffusion-based image-

to-image translation model, adept at addressing data imbalance. Finally, in the alopecia severity assessment phase, we utilize hair masks to derive features like hair thickness and count, which are then analyzed using machine learning models to provide accurate evaluations.

In summary, our main contributions are as follows:

- We present a comprehensive diagnostic pipeline for microscopic scalp imagery that assesses both scalp condition and alopecia severity.
- We develop a novel segmentation approach, combining heuristic-driven pseudo-labels with SAM to effectively segment images in the absence of ground truth labels.
- We introduce DiffuseIT-M, a mask-guided, diffusion-based image-to-image translation method, facilitating targeted control over specific image regions without additional training.

We contribute to the field of scalp diagnosis by sharing our code on GitHub².

2. Related Works

Scalp image analysis. In the field of scalp image analysis, hair is a pivotal feature, often utilized for segmentation purposes [44, 48]. Investigations into the number [41, 52] and thickness [23] of hairs on microscopic scalp images have been conducted. Moreover, various approaches utilize microscopic scalp images to diagnose diseases. Systems for classifying scalp diseases and their severity have been developed [7, 25], while others assess alopecia severity using scalp information [24, 43].

Image augmentation. Previous studies have proposed methods for data augmentation by merging images [53, 54]

¹This dataset is provided by ‘The Open AI Dataset Project (AI-Hub, S. Korea)’ and is exempt from IRB approval as it does not contain any information that can identify individuals.

²<https://github.com/winston1214/ScalpVision>

or losing partial information of images [8, 58]. Recent developments in generative models, particularly the diffusion models [20, 40], have led to the proposal of image augmentation methods using synthetic images. Azizi and Trabucco *et al.* [3, 47] show diffusion models can generate photo-realistic images with given conditioning variables and improve image classification accuracy, even in medical applications [11, 57].

Label-free image segmentation on medical image. The challenges and expenses associated with acquiring medical image data have spurred the development of data-efficient training methods [9] and label-free segmentation models. Kim *et al.* [22] introduced a synthetic angiogram based on fractal design as a label, training a diffusion module for vessel segmentation. Large pre-trained segmentation models like the Segment Anything Model (SAM) [26] have garnered interest and demonstrated promise across various vision tasks [59]. While these models are increasingly applied to specific medical imaging challenges, success has been limited [17].

3. Our Approach: ScalpVision

To address the challenges of limited and imbalanced datasets in scalp imaging, we introduce ScalpVision, a diagnostic system designed for accurately assessing the severity of scalp-related diseases and alopecia. Central to ScalpVision is a hair segmentation module (Section 3.1), pivotal for both alopecia severity prediction (Section 3.2) and generating diverse scalp images to augment training datasets for scalp condition classification (Section 3.3). The overall pipeline of ScalpVision is illustrated in Figure 2.

3.1. Label-Free Hair Segmentation

For the precise diagnosis of alopecia and scalp conditions, our initial step involves segmenting hair within microscopic scalp images. However, as the dataset does not provide explicit segmentation labels, conventional supervised learning methods are not feasible.

Heuristic-driven pseudo-labeling. To address this, we first generate pseudo labels for training our segmentation model (S as shown in Figure 2) using prior knowledge. With the intuition that the hair on the microscopic scalp images follows either a linear function or a power function, we generate synthetic images to effectively guide the model to learn hair patterns on the scalp images. For each disease condition, we randomly select one image representing each distinct severity level, extract three smaller patches from regions of the scalp with no visible hair, and draw curves to simulate hair patterns. Additionally, to simulate dandruff noise, circular white shapes are added to these patches, but are not indicated in the pseudo masks, thus training the model to interpret them as noise. We generate 3,000 pseudo-images and corresponding pseudo mask labels, us-

Algorithm 1 Extraction of representative points from mask

Input: Mask \hat{M} , bounding box size n , and cross-shaped structuring element $kernel$

Output: Representative hair points from mask \hat{C}

```

1:  $\mathcal{H}_{copy} \leftarrow \hat{M}$ 
2:  $\hat{\mathcal{H}}_{skel} \leftarrow$  zero array with same size as  $\mathcal{H}_{copy}$ 
3: while  $\mathcal{H}_{copy} \neq 0$  do
4:    $Eroded, Dilated \leftarrow$  MORPHOLOGY( $\mathcal{H}_{copy}, kernel$ )
5:    $\hat{K} \leftarrow \mathcal{H}_{copy} - Dilated$ 
6:    $\hat{\mathcal{H}}_{skel} \leftarrow \hat{\mathcal{H}}_{skel} \vee \hat{K}$ 
7:    $\mathcal{H}_{copy} \leftarrow Eroded$ 
8: end while
9:  $\hat{B} \leftarrow \{\}$ 
10: for all  $(x, y) \in \mathcal{H}_{skel}$  do
11:    $\hat{B} \leftarrow \hat{B} \cup \{(x - \frac{1}{2}n, y - \frac{1}{2}n, x + \frac{1}{2}n, y + \frac{1}{2}n)\}$ 
12: end for
13:  $\hat{B} \leftarrow$  NMS( $\hat{B}$ )
14:  $\hat{C} \leftarrow \{\}$ 
15: for all  $(x_1, y_1, x_2, y_2) \in \hat{B}$  do
16:    $\hat{C} \leftarrow \hat{C} \cup \{(\bar{x}, \bar{y})\}$  as in Eq.(2)
17: end for
18: return  $\hat{C}$ 

```

ing them to train the U²-Net [39]. This training generates the binary mask, represented as:

$$\hat{M} = [\hat{M}(i, j)] \in \{0, 1\}^{H \times W}, \quad (1)$$

where H and W are the height and width of the image, and $i \in [1, H], j \in [1, W]$ denote pixel coordinates.

Automatic prompting for SAM. To refine the hair segmentation mask \hat{M} , we utilize the foundation segmentation model, SAM [26], employing a point-prompting method to differentiate hair from scalp without additional training. However, we observed that selecting random points from \hat{M} for positive point prompts often resulted in suboptimal masks. This issue was primarily due to points near the edges of \hat{M} causing confusion for the SAM. Moreover, due to inherent randomness, there were instances in which sampled points clustered in a small localized region, resulting in the SAM segmenting only a limited number of hairs. To address these issues, we have developed an automatic prompting method. This method ensures uniform sampling across \hat{M} and provides high-confidence guidance to the SAM based on the coarse segmentation mask \hat{M} . The specific steps of this method are detailed in Algorithm 1.

To extract the distinct features of the hair, we compute the skeletonized mask $\hat{\mathcal{H}}_{skel} (\in \{0, 1\}^{H \times W})$ using morphological erosion and dilation following [56]. This method operates by iteratively processing the image, eroding and dilating pixels at the object’s edges until no further pixel removal is possible. Then, we generate bounding boxes around each pixel in $\hat{\mathcal{H}}_{skel}$ with size $n \times n$ where we set $n = 10$. These boxes undergo non-maximum suppression (NMS) to filter out the bounding boxes, denoted as

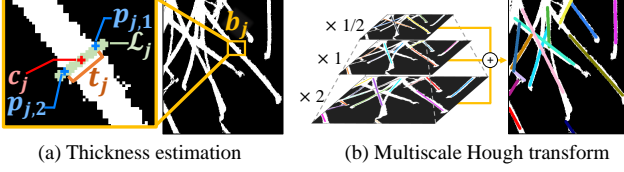


Figure 3. Feature extraction for alopecia severity prediction.

$\hat{B} = \{\hat{b}_j\}_{j=1}^k$, where each box is defined by coordinates $(x_{\min}, y_{\min}, x_{\max}, y_{\max})$. Following this, the mean points of the hair pixels, $\hat{C} = \{\hat{c}_j\}_{j=1}^k$, in each bounding box \hat{B} can be determined. For each $\hat{b}_j = (x_1, y_1, x_2, y_2)$, the mean point $\hat{c}_j = (\bar{x}, \bar{y})$ is given by:

$$\bar{x} = \frac{\sum_i \sum_j i \cdot \hat{\mathcal{H}}(i, j)}{\sum_i \sum_j \hat{\mathcal{H}}(i, j)}, \quad \bar{y} = \frac{\sum_i \sum_j j \cdot \hat{\mathcal{H}}(i, j)}{\sum_i \sum_j \hat{\mathcal{H}}(i, j)} \quad (2)$$

where the summation is over all $i \in [x_1, x_2]$ and $j \in [y_1, y_2]$.

Subsequently, we select positive point prompts for SAM from the calculated mean points \hat{C} . For the negative point prompts, we utilize the inverse of the initial mask, specifically $1 - \hat{M}$. These prompts, automatically generated, guide SAM in generating the binary segmentation mask $M_{AP} \in \{0, 1\}^{H \times W}$.

Mask ensemble. M_{AP} and \hat{M} complement each other with strengths and weaknesses. \hat{M} is robust against noise like dandruff as it was trained using simulated noise. Meanwhile, M_{AP} , benefiting from SAM’s superior edge detection, excels in constructing a clear boundary between hair and scalp. Therefore, to make a robust hair mask, the final binary mask, M , is derived from \hat{M} and M_{AP} with the AND operation, as follows:

$$M = \hat{M} \wedge M_{AP}. \quad (3)$$

3.2. Alopecia Severity Prediction

Alopecia primarily manifests through two indicators: hair thinning and follicle reduction [38]. Consequently, hair thickness and count are crucial metrics for assessing its severity. However, lacking ground-truth labels for these features, we have developed straightforward yet effective methods to approximate hair thickness (Figure 3(a)) and hair count (Figure 3(b)). These methods utilize the hair mask M generated earlier, from which we extract bounding boxes B , and their respective mean points C , following the approach described in Section 3.1.

Hair thickness. Our objective is to measure the thickness of hair within each bounding box in the set $B = \{b_j\}_{j=1}^k$. Firstly, we define the set of pixel coordinates for hair within a bounding box b_j as:

$$\mathcal{P}_j = \{(x, y) \in b_j \mid M(x, y) = 1\}, \quad (4)$$

where $M(x, y) = 1$ indicates the presence of hair at the pixel coordinates (x, y) .

Next, we calculate $\mathcal{S} = \{s_j\}_{j=1}^k$ where each s_j represents the slope perpendicular to the hair in the j -th bounding box. This slope is derived from the second principal component in a Principal Component Analysis (PCA) of the pixel coordinates \mathcal{P}_j . A perpendicular line (\mathcal{L}_j) is then defined using this slope s_j and the mean point c_j :

$$\mathcal{L}_j = \{(x, y) \mid s_j(x - c_{j,x}) + c_{j,y} = y\}. \quad (5)$$

Following this, we identify two boundary points of the hair, $p_{j,1}$ and $p_{j,2}$, located where \mathcal{L}_j intersects with the edge points of \mathcal{P}_j . Denoting these edge points as $E(\mathcal{P}_j)$, the boundary points are formulated as:

$$p_{j,1}, p_{j,2} = E(\mathcal{P}_j) \cap \mathcal{L}_j. \quad (6)$$

Finally, the pixel-level hair thickness (t_j) is calculated as the Euclidean distance between these two boundary points:

$$t_j = \|p_{j,1} - p_{j,2}\|_2. \quad (7)$$

Thus, we obtain a set of hair thicknesses: $\mathcal{T} = \{t_j\}_{j=1}^k$.

Hair count. To quantify the number of hairs, we utilize the Hough transformation [13], an established technique for line detection through parameter space representation, applied to the hair skeleton $\mathcal{H}_{\text{skel}}$. Inspired by the approach in [45], we enhance the method’s effectiveness for curved hair by implementing the Hough transformation at three different resolutions: original, half, and double. At each of these resolutions, the transformation identifies a set of line segments, where each segment is defined by a pair of endpoints, denoted as $\{(x_1, y_1), (x_2, y_2)\}$. The line segments obtained from each resolution level are then resized to correspond to the original resolution scale and collectively merged. During this merging phase, we identify and remove duplicate line segments. This elimination is based on their similarity in vector angle, length, and spatial positioning.

The two features we have predicted, hair thickness and count, not only hold potential for direct use by clinicians in diagnosing alopecia but also present an opportunity for further exploration. Considering the dataset includes labels on the severity of alopecia, we investigate the application of these features as inputs for traditional machine learning models. This approach is aimed at enhancing the prediction of alopecia severity using the available dataset.

3.3. Scalp Condition Classification

Accurately classifying the severity of scalp-related diseases in microscopic images is challenging due to the rarity of extreme cases, as illustrated in Figure 1. To address this issue, we have developed a method that translates given images into scalp images of a desired condition. This method,

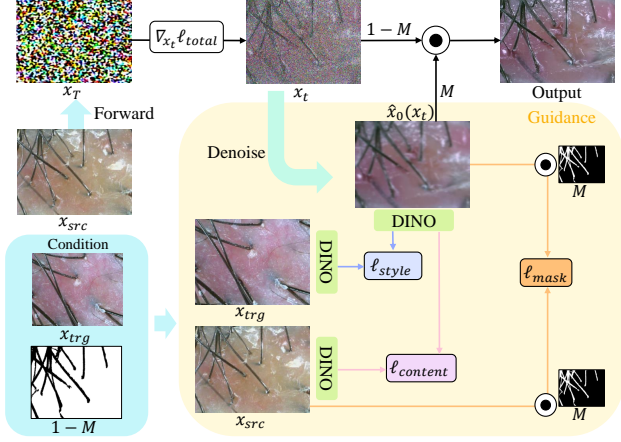


Figure 4. Overview of DiffuseIT-M. x_{src} and x_{trg} represent the source image and target image, respectively, with M denoting the mask image of x_{src} . In the reverse process, we guide the generation to adhere to the conditions using the objective function. \odot signifies the weighted sum of two images. “DINO” means DINO-ViT.

named DiffuseIT-M, is a diffusion-based image translation model with mask guidance. It is designed to preserve the content (e.g., hair) of the source image while enabling the transformation into various scalp conditions. DiffuseIT-M is based on DiffuseIT [27] and incorporates an image editing technique inspired by Blended diffusion [2] to ensure hair preservation. The overview of DiffuseIT-M is depicted in Figure 4.

Preliminary. In the forward diffusion process, we adopted the DDPM [20] forward process. Given a clean image, $x_0 \sim q(x_0)$, Gaussian noise is gradually added at every time steps, t , using the Markov chain.

$$q(x_{1:T}|x_0) := \prod_{t=1}^T q(x_t|x_{t-1}), \quad (8)$$

following the formulations and notations in [33]. This equation can be simplified in terms of x_t sampled in one step as follows:

$$x_t = \sqrt{\bar{\alpha}_t}x_0 + \sqrt{1 - \bar{\alpha}_t}\epsilon, \quad (9)$$

where $\epsilon \sim \mathcal{N}(0, \mathbf{I})$, $\alpha_t := 1 - \beta_t$ and $\bar{\alpha}_t := \prod_{s=1}^t \alpha_s$.

In the reverse diffusion process, $q(x_{t-1}|x_t)$ is approximated as $p_\theta(x_{t-1}|x_t)$ with the trainable parameter θ . Therefore, it is modeled by a Markov chain with a learned mean and fixed variance, initiated from $p(x_T)$:

$$p_\theta(x_{0:T}) := p_\theta(x_T) \prod_{t=1}^T p_\theta(x_{t-1}|x_t) \quad (10)$$

where $p_\theta(x_{t-1}|x_t) := \mathcal{N}(x_{t-1}; \mu_\theta(x_t, t), \Sigma_\theta(x_t, t))$. Rather than inferring $\mu_\theta(x_t, t)$ directly, it predicts the noise

$\epsilon_\theta(x_t, t)$ added to x_0 to obtain x_t . Then, $\mu_\theta(x_t, t)$ is derived using Bayes’ theorem:

$$\mu_\theta(x_t, t) = \frac{1}{\sqrt{\alpha_t}} \left(x_t - \frac{1 - \alpha_t}{\sqrt{1 - \bar{\alpha}_t}} \epsilon_\theta(x_t, t) \right). \quad (11)$$

Then, the sampling from the reverse diffusion is defined as:

$$x_{t-1} = \mu_\theta(x_t, t) + \sigma_t \epsilon. \quad (12)$$

Image translation with mask guidance. To facilitate the transfer of scalp disease characteristics while preserving hair features in our model, we utilize a comprehensive loss function, ℓ_{total} . This function guides the reverse process and is composed of five distinct loss components. These components consider the source image (x_{src}), the target image (x_{trg}), and the hair mask (M) as inputs. The combined loss function is defined as:

$$\ell_{total}(x; x_{src}, x_{trg}, M) = \lambda_1 \ell_{style} + \lambda_2 \ell_{content} + \lambda_3 \ell_{mask} + \lambda_4 \ell_{sem} + \lambda_5 \ell_{rng}, \quad (13)$$

where $\lambda_{i \in [1,5]}$ denotes the weights assigned to each of these loss functions.

For ℓ_{style} and $\ell_{content}$, we utilize the style and content loss functions from DiffuseIT. We employ the [CLS] token matching loss using DINO ViT [6] to reflect semantic information in x_{trg} and use keys of multi-head self-attention layers to preserve the content of x_{src} .

Additionally, to ensure hair preservation while translating scalp styles, we construct mask preservation loss function as:

$$\ell_{mask} = LPIPS(x_{src} \odot M, \hat{x}_0(x_t) \odot M) + \|(x_{src} - \hat{x}_0(x_t)) \odot M\|_2, \quad (14)$$

where $LPIPS$ denotes the learned perceptual image patch similarity metric [55].

We also include two other loss functions: ℓ_{rng} , representing the squared spherical distance as proposed in [10], and ℓ_{sem} , indicating the semantic divergence loss as outlined in [27].

Using this composite loss function, ℓ_{total} , we guide the generation of the next sample step, x_{t-1} . To maintain hair information, we apply masking to the images:

$$x_{t-1} = x_t \odot (1 - M) + \left(\hat{x}_0(x_t) - \nabla_{x_t} \ell_{total}(\hat{x}_0(x_t)) \right) \odot M, \quad (15)$$

where $\hat{x}_0(x_t)$ is the estimation of the cleaned image derived from the sample x_t . This estimation is computed as follows:

$$\hat{x}_0(x_t) = \frac{x_t}{\sqrt{\alpha_t}} - \frac{\sqrt{1 - \bar{\alpha}_t} \epsilon_\theta(x_t, t)}{\sqrt{\bar{\alpha}_t}}. \quad (16)$$

With this guide, we can translate the image style of the scalp without the need for additional training.

Classification strategy. Utilizing our DiffuseIT-M, as described above, we enhance our training set by translating randomly chosen images into ones with higher severity levels. We used random selection for the source images and weighted sampling for target images, where the likelihood of choosing an image was inversely proportional to the number of samples in its severity class.

For our classification task, we employed a pretrained backbone model and fine-tuned it with four Multi-Layer Perceptron (MLP) heads. Each head is associated with a specific loss function. The first head is designed to identify the presence of each scalp disease (*i.e.*, *dandruff*, *excess sebum*, and *erythema*) without considering their severity. The remaining three heads are tasked with classifying the severity levels of each disease, categorized into four stages: *good*, *mild*, *moderate*, and *severe*. Consequently, our overall classification objective, denoted as ℓ_{cls} , is expressed by the following formula:

$$\ell_{cls} = \ell_{dis} + \ell_{dand} + \ell_{seb} + \ell_{ery}, \quad (17)$$

where ℓ_{dis} is the binary cross-entropy loss for the disease presence classification head, and ℓ_{dand} , ℓ_{seb} , and ℓ_{ery} represent the cross-entropy losses associated with determining the severity levels of each disease.

4. Experiments

To showcase the effectiveness of our pipeline, we conducted a series of quantitative and qualitative experiments for each component of the pipeline.

4.1. Dataset

We trained and evaluated our model using the scalp image dataset from AI-Hub [1], previously mentioned in Section 1 and depicted in Figure 1. The dataset comprises 95,910 images with a resolution of 640×480 pixels from 20,000 patients. It is divided into 72,342 images for training and 23,568 images for testing, with a subset of 21,703 images from the training set designated for validation. Dermatologists classified these scalp images into one or more of the following conditions: *dandruff*, *excess sebum*, and *erythema*. Each condition was further assessed for severity, categorized as *mild*, *moderate*, or *severe*, with an additional category, *good*, indicating no presence of the condition. Furthermore, a subset of 23,803 images, divided into 12,902 for training, 5,613 for validation, and 5,288 for testing, includes specific labels for alopecia severity, following the same four-level categorization.

4.2. Hair Segmentation

To evaluate the performance of the hair segmentation methods, we manually annotated hair regions in 150 images from the test set. For baseline methods, we selected previous

Table 1. Performance of Hair segmentation on manually annotated test set.

Approach		Pixel-F1	Jaccard	Dice
Shih <i>et al.</i> [44]		0.7063	0.3475	0.5119
Yue <i>et al.</i> [52]		0.7943	0.4933	0.6540
Kim <i>et al.</i> [23]		0.8150	0.5614	0.7078
SAM [26]		0.5030	0.3609	0.5024
Ours	\hat{M}	0.8534	0.6039	0.7481
	M_{AP}	0.8358	0.5951	0.7429
	M	0.8680	0.6494	0.7859

studies related to scalp image analysis [23, 44, 52] and SAM [26]. Additionally, we performed an ablation study comparing our final segmentation result (M) with the intermediate results (\hat{M} and M_{AP}).

Quantitative results. Table 1 reveals that our methods surpass the performance of existing hair segmentation techniques. In particular, the approach of combining the advantages of the two masks, \hat{M} and M_{AP} using the AND operator in M showed the best performance. These results show the limitations of traditional computer vision techniques used in previous studies for image segmentation, revealing a lack of understanding in capturing the intricate patterns of hair and the scalp. Additionally, we observed that SAM, when used without specific guidance, was less effective for automatic image segmentation.

Qualitative results. As shown in Figure 5, our approach demonstrates effective hair segmentation with robustness to noise, providing clear and accurate hair segmentation compared to previous methods. Furthermore, it shows that \hat{M} faces challenges in clearly capturing hair, and it exhibits robustness against noise such as dandruff. Conversely, M_{AP} captures the hair well but is less robust to noise. Therefore, the combination of the two masks, M , demonstrates the mitigation of the drawbacks of each mask.

4.3. Scalp Disease and Severity Diagnosis

Synthetic image generation. For the evaluation of DiffuseIT-M, we compared our model against DiffuseIT [27] and AGG [28] as baseline for the state-of-the-art image-to-image translation model. We have selected to employ the FID [19] and LPIPS [55] scores for fidelity evaluation. Comparative experiments were conducted using images from our augmentation dataset, with DiffuseIT and AGG serving as baseline models. Table 3 reveals that DiffuseIT-M outperforms other models in both metrics, indicating superior image fidelity. This high-quality image generation is attributed to our model’s effective implementation of mask guidance. As shown in Figure 6, we can observe that both DiffuseIT and AGG models fail to pre-

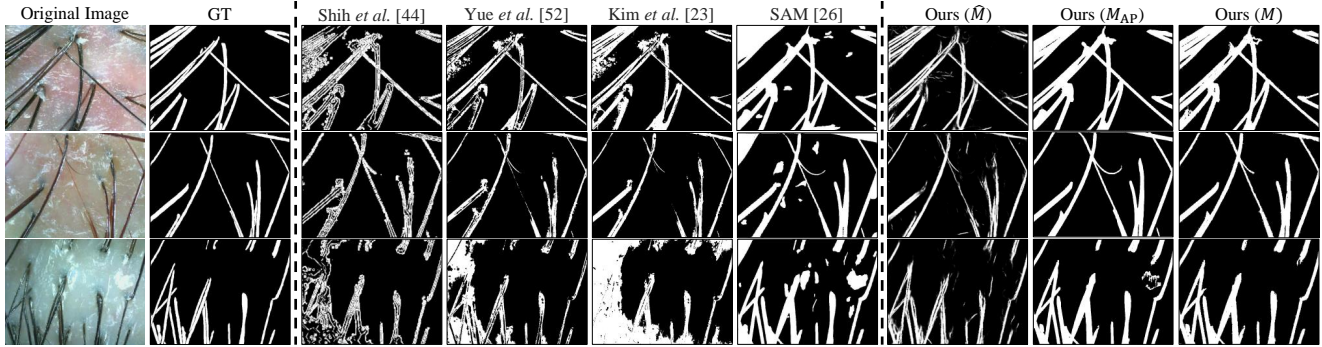


Figure 5. Comparison of various segmentation methods on hair. “GT” represents the mask images for which we have manually annotated the pixel segmentation. Note that \hat{M} , M_{AP} and M are proposed in Section 3.1.

Table 2. Performance of scalp condition classification with various augmentation methods, denoted after “+” symbol, on the test set. The second column displays the overall macro-F1 score, while the third to last column shows the F1 scores for each severity level of three diseases.

Model	F1	Dandruff				Sebum				Erythema			
	macro	good	mild	moderate	severe	good	mild	moderate	severe	good	mild	moderate	severe
DenseNet [21]	0.5819	0.7962	0.5140	0.5916	0.6138	0.5541	0.6013	0.6412	0.0000	0.7758	0.7287	0.5652	0.6010
+ Gaussian Noise	0.5667	0.7804	0.4969	0.5662	0.5971	0.4712	0.5809	0.5946	0.0000	0.7509	0.7119	0.6142	0.6352
+ AugMix [18]	0.5249	0.7886	0.5009	0.5890	0.0000	0.5042	0.5882	0.6341	0.0000	0.7430	0.7179	0.5956	0.5845
+ DiffuseIT [27]	0.6079	0.8090	0.4824	0.6041	0.6500	0.5357	0.6126	0.6245	0.2024	0.7744	0.7395	0.6209	0.6388
+ AGG [28]	0.6103	0.8106	0.4803	0.5908	0.6539	0.5175	0.5977	0.6119	0.2997	0.7713	0.7402	0.6291	0.6206
+ Ours	0.6358	0.8196	0.5407	0.6253	0.6652	0.5362	0.6174	0.6414	0.4296	0.7578	0.7339	0.6214	0.6412
EfficientFormerV2 [30]	0.5692	0.7954	0.4172	0.5983	0.6279	0.5257	0.5648	0.6283	0.0000	0.7722	0.7090	0.6227	0.5685
+ Gaussian Noise	0.5618	0.7799	0.4774	0.5658	0.6326	0.4601	0.5850	0.5501	0.0000	0.7418	0.7141	0.5980	0.6372
+ AugMix [18]	0.5770	0.7885	0.4940	0.5916	0.6347	0.5189	0.5927	0.6228	0.0000	0.7460	0.7238	0.6199	0.5904
+ DiffuseIT [27]	0.5955	0.7981	0.4410	0.5977	0.6316	0.5263	0.5953	0.6057	0.2362	0.7658	0.7149	0.6121	0.6214
+ AGG [28]	0.6098	0.8012	0.5087	0.6037	0.6262	0.5112	0.5830	0.6084	0.2999	0.7874	0.7364	0.6239	0.6275
+ Ours	0.6346	0.8066	0.5290	0.6190	0.6689	0.5345	0.6129	0.6324	0.4060	0.7811	0.7382	0.6394	0.6476

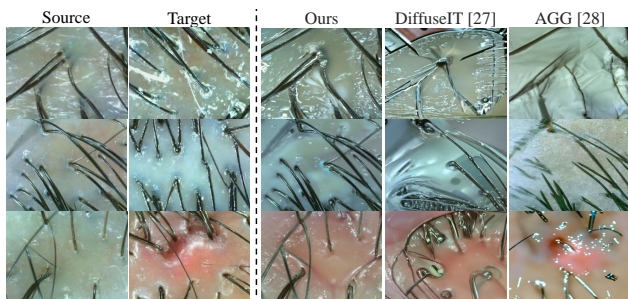


Figure 6. Image translation results with different generative models. The goal is to maintain the content of the source image while translating the scalp condition to the target image.

serve the hair content information from the source image. Furthermore, these models tended to compromise overall information and were unable to transfer the semantic information. However, our model successfully preserved hair content information and transferred the semantic information.

Effect of mask guidance. We conducted experiments to

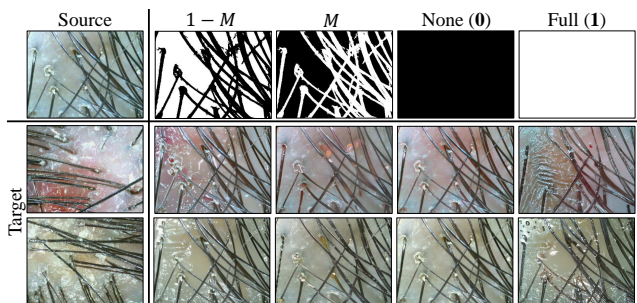


Figure 7. Image translation results using various mask guidance. Note that our approach is guided by $1 - M$.

examine the impact of mask guidance on hair information preservation during image translation. As illustrated in Figure 7, our method, guided by the mask $1 - M$, effectively retains hair features while successfully transferring the semantic attributes of the target image onto the scalp. In contrast, using the reverse mask, M , leads to only minor alterations in scalp color from the target image, with a notable transfer of hair semantic information from the target. When

Table 3. Quantitative analysis of image-to-image translation performance.

Model	FID (\downarrow)	LPIPS (\downarrow)
DiffuseIT [27]	138.42	0.4631
AGG [28]	141.70	0.4915
Ours	74.84	0.3528

Table 4. Performance of alopecia severity classification.

	Method	Accuracy	Weighted F1
Image-Based	DenseNet [51]	0.6686	0.6283
	EfficientFormerV2 [12]	0.6728	0.6351
Feature-Based	Kim <i>et al.</i> [23]	0.5994	0.6062
	Ours	0.7460	0.6873

no mask (0) is applied, the translation results in minimal color change, failing to transfer conditions like dandruff from the target image. Conversely, with a full mask (1), both hair and scalp features are subjected to changes. This differentiation in results highlights the importance of mask guidance in preserving specific image features, demonstrating the versatility of our approach in handling different translation objectives.

Scalp condition classification. To demonstrate the effectiveness of our augmentation method using generated images, we employed two different models as the classification backbone: DenseNet [21] as a CNN and EfficientFormerV2 [30] as a Transformer. We conducted a comparative analysis with other augmentation methods, including the addition of Gaussian noise, AugMix [18], DiffuseIT [27], and AGG [28]. The results are summarized in Table 2.

Our approach, specifically employing DiffuseIT-M, achieved the highest performance in both models. Notably, classifying the *severe* sebum class proved to be especially challenging when using non-generative augmentation methods. This difficulty arises primarily due to the extreme scarcity of samples for this class. The augmentation of the training dataset with generative models led to enhanced performance compared to the baseline, thanks to the effective style and content guidance from these models. Our model, in particular, exhibited superior accuracy compared to DiffuseIT and AGG, which struggled to preserve the essential information of the hair effectively. This underscores the significance of incorporating both the scalp style details and the hair content information in scalp disease classification.

4.4. Alopecia Severity Diagnosis

To diagnose the severity of alopecia, we utilized hair-related features such as hair thickness and count, as described in Section 3.2. These features were then employed to make



Figure 8. Distribution of features used for alopecia prediction. This figure illustrates the distribution of \mathcal{T} , representing hair thickness values, and $|B|$, indicating the count of bounding boxes in each image.

predictions using a GradientBoosting model [15].

Our method was benchmarked against both image-based and traditional feature-based diagnostic approaches. For image-based severity prediction, we used DenseNet and EfficientFormerV2 models as baselines, which directly analyze the images to predict alopecia severity. Conversely, for feature-based prediction, we employed a method from [23], which involves generating masks through Otsu-based thresholding [34] and extracting features based on average hair thickness.

Since the data on alopecia severity is imbalanced, as shown in Figure 1, we selected to use both accuracy and weighted F1-score as evaluation metrics.

Alopecia severity classification. Our approach consistently outperforms other methods, including those based on image analysis, as shown in Table 4. This highlights the significance of hair thickness and counts as key diagnostic features for alopecia and validates the accuracy of our method in predicting these attributes precisely.

Feature distribution. We analyzed the distribution of input features across different alopecia severity levels. As illustrated in Figure 8, box plots for each feature show a consistent decrease from the *good* to *severe* categories. This trend indicates that our balanced sample set allowed each feature to contribute effectively to the severity prediction, enhancing the model’s accuracy.

5. Ablation Studies

5.1. Automatic Prompting for SAM

We conducted an ablation study to evaluate our automatic prompting method with SAM. The study comprised four different approaches: 1) positive point prompts from \hat{M} and negative point prompts from $1 - \hat{M}$, 2) positive point

Table 5. Comparative analysis of different prompting methods with SAM. The symbol “-” indicates scenarios where no prompt was used.

Positive	Negative	Pixel-F1	Jaccard	Dice
\hat{M}	$1 - \hat{M}$	0.3786	0.1199	0.1891
\hat{H}_{skel}	$1 - \hat{M}$	0.8210	0.5707	0.7215
\hat{C}	-	0.4966	0.2754	0.4148
\hat{C}	$1 - \hat{M}$	0.8358	0.5951	0.7429

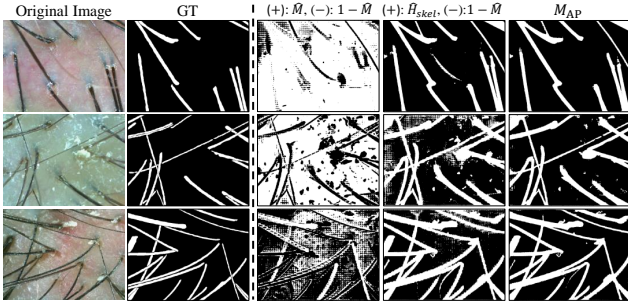


Figure 9. Illustration of hair segmentation results using different prompt guides. “GT” represents segmentation guided by the ground truth mask, while M_{AP} signifies our final prompting method with positive prompts from \hat{C} and negative prompts from $(1 - \hat{M})$. “(+)” refers to positive prompts and “(-)” refers to negative prompts.

prompts from \hat{H}_{skel} and negative point prompts from $1 - \hat{M}$, 3) positive point prompts from \hat{C} without negative prompts, and 4) positive prompt points from \hat{C} and negative point prompts from $1 - \hat{M}$ (**Ours**).

Quantitative results. Table 5 demonstrates that our method outperforms the others across all metrics. Notably, the absence of negative prompts significantly diminishes performance, underscoring their importance in the model.

Qualitative results. Figure 9 showcases the efficacy of our point prompting method in hair segmentation. While using \hat{H}_{skel} for prompting improves over \hat{M} , it often results in unevenly distributed sampled points, leading to a noisier mask than that produced by our method.

5.2. Hair Preservation Efficacy in Generative Models

We conducted an analysis to understand how various image-to-image generative models impact hair segmentation. Specifically, we transformed 150 test images by applying a healthy target image (devoid of any scalp diseases) using three different generative models. We then applied our segmentation method to these images for a thorough quantitative evaluation.

Quantitative results. For a numerical evaluation of hair preservation, we generated images and then applied seg-

Table 6. Comparative analysis of hair segmentation across different generative methods.

Model	Pixel-F1	Jaccard	Dice
DiffuseIT	0.7106	0.3619	0.5153
AGG	0.7286	0.3785	0.5403
Ours (M)	0.7625	0.4485	0.6067
Ours (GT)	0.7812	0.4840	0.6416

Table 7. Ablation study of impact analysis of features in the alopecia severity prediction. HC is the number of Hair estimation from Section 3.2, \mathcal{T} is the list of hair thickness estimations and $|B|$ is the number of bounding boxes in an image. The “ $\tilde{\mathcal{T}}$ ” symbol denotes the median of \mathcal{T} , while the “ $\bar{\mathcal{T}}$ ” symbol signifies the mean of \mathcal{T} . An “*” symbol signifies that outliers were removed. The order in which features are added reflects feature importance in the final model.

HC	$\tilde{\mathcal{T}}^*$	$\tilde{\mathcal{T}}$	$ B $	$\bar{\mathcal{T}}$	$\bar{\mathcal{T}}^*$	Accuracy	F1 (Weighted)
✓						0.7233	0.6109
✓	✓					0.7369	0.6650
✓	✓	✓				0.7390	0.6712
✓	✓	✓	✓			0.7407	0.6761
✓	✓	✓	✓	✓		0.7436	0.6783
✓	✓	✓	✓	✓	✓	0.7460	0.6873

mentation metrics like pixel F1, Jaccard index, and Dice score. Table 6 showcases the results, highlighting that DiffuseIT-M (denoted as Ours (M)) excels in preserving hair details, thereby affirming its efficacy in retaining essential content from the source images. Moreover, we examined the segmentation outcomes when using GT masks (denoted as Ours (GT)) alongside our model. This comparison illustrated that improving mask quality significantly enhances the preservation of hair features in the generated images, providing insights into how mask quality impacts hair content retention in generative models.

Qualitative results. We compared hair preservation in images generated by our model with those from other models. Our model used GT masks as guides during the generation process. Figure 10 shows the hair segmentation results for images generated by our model alongside the GT masks. The comparison demonstrates that our model effectively retains hair content from source images, unlike DiffuseIT and AGG, which struggled to maintain comprehensive hair details. In particular, AGG tended to preserve only dominant hair features, omitting finer details.

5.3. Feature Selection for Severity Estimation

We identified key features for alopecia severity prediction, focusing on hair thickness and count. For thickness, we

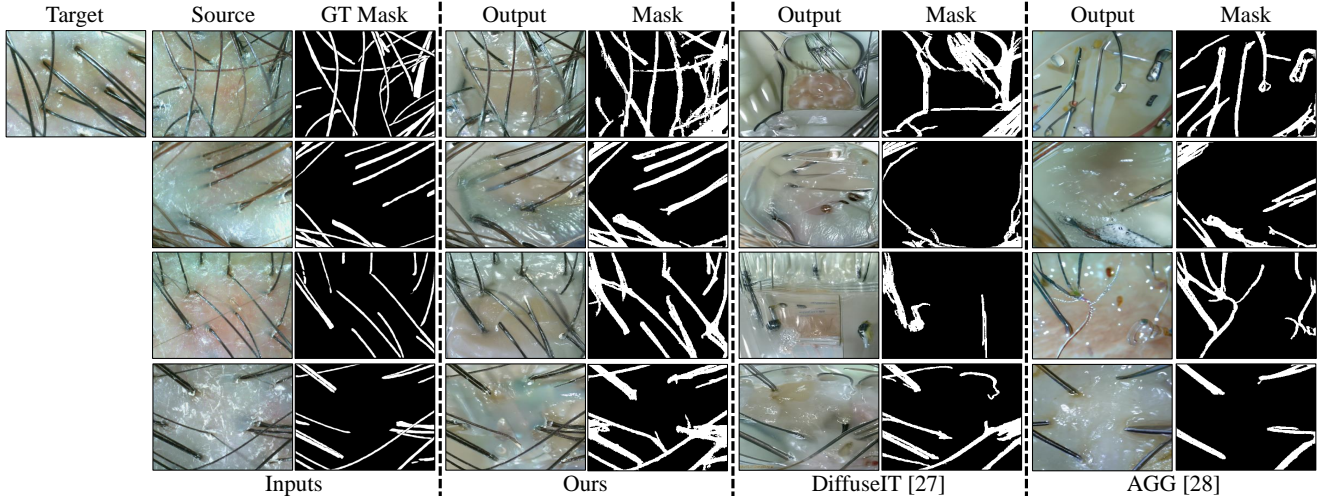


Figure 10. Comparative qualitative results of hair segmentation across different generative models.

analyzed the length of the list B and computed the mean and median values of \mathcal{T} , excluding outliers identified using the interquartile range (IQR). We also considered the mean and median of the entire \mathcal{T} . Additionally, the number of line segments detected by the hair count estimator was used as a supplementary feature.

Feature importance. An analysis using the GradientBoosting model (Table 7) revealed that the best prediction accuracy was achieved when all features were combined. This finding underscores the significance of each extracted feature in our model.

6. Conclusion

In this work, we introduced ScalpVision, diagnostic system designed for a complete evaluation of scalp health. This system harnesses label-free learning combined with a foundational model to create precise hair segmentation masks. Additionally, ScalpVision employs diffusion-based image augmentation for accurate scalp condition diagnosis and leverages estimations of hair thickness and count to assess alopecia severity. We envision ScalpVision as a significant step towards a generalized diagnostic system for dermatological applications, particularly in simplifying the challenges associated with complex labeling in microscopic scalp imaging.

7. Limitation

There are several limitations of ScalpVision that would make for promising avenues of future work, which mainly stems from dataset constraints. The limited labels in the dataset pose challenges in accurately diagnosing scalp and alopecia conditions. For example, while follicle count is crucial for alopecia diagnosis, we used hair count as a proxy

due to data limitations. However, not all visible hairs in an image necessarily originate from follicles within the same image, making this a less than ideal substitute. Additionally, we assumed that scalp images capture a consistent area. In reality, slight variations in the distance from which images are captured can lead to differences in perceived hair thickness. Addressing these discrepancies requires further research into standardizing image capture methods or developing models robust to such variations.

Acknowledge

This work was partly supported by an IITP grant (No. RS-2020-II201361, RS-2022-00155966) and NRF grant (No. RS-2024-00354218) funded by the Korea government (MSIT).

References

- [1] AI Hub. Scalp and Hair Follicle Image Dataset, 2020. [Online; accessed 9 February 2023]. 2, 6
- [2] Omri Avrahami, Dani Lischinski, and Ohad Fried. Blended diffusion for text-driven editing of natural images. In *Proceedings of the IEEE/CVF Conference on Computer Vision and Pattern Recognition*, pages 18208–18218, 2022. 5
- [3] Shekoofeh Azizi, Simon Kornblith, Chitwan Saharia, Mohammad Norouzi, and David J. Fleet. Synthetic data from diffusion models improves imagenet classification, 2023. 3
- [4] Luis J Borda and Tongyu C Wikramanayake. Seborrheic dermatitis and dandruff: a comprehensive review. *Journal of clinical and investigative dermatology*, 3(2), 2015. 1
- [5] Lars Buitinck, Gilles Louppe, Mathieu Blondel, Fabian Pedregosa, Andreas Mueller, Olivier Grisel, Vlad Niculae, Peter Prettenhofer, Alexandre Gramfort, Jaques Grobler, Robert Layton, Jake VanderPlas, Arnaud Joly, Brian Holt, and Gaël Varoquaux. API design for machine learning software: experiences from the scikit-learn project. In *ECML PKDD Workshop: Languages for Data Mining and Machine Learning*, pages 108–122, 2013. 2
- [6] Mathilde Caron, Hugo Touvron, Ishan Misra, Hervé Jégou, Julien Mairal, Piotr Bojanowski, and Armand Joulin. Emerging properties in self-supervised vision transformers. In *Proceedings of the IEEE/CVF international conference on computer vision*, pages 9650–9660, 2021. 5, 1
- [7] Wan-Jung Chang, Liang-Bi Chen, Ming-Che Chen, Yi-Chan Chiu, and Jian-Yu Lin. Scalpeye: A deep learning-based scalp hair inspection and diagnosis system for scalp health. *IEEE Access*, 8:134826–134837, 2020. 1, 2
- [8] Pengguang Chen, Shu Liu, Hengshuang Zhao, and Ji-aya Jia. Gridmask data augmentation. *arXiv preprint arXiv:2001.04086*, 2020. 3
- [9] Ouyang Cheng, Konstantinos Kamnitsas, Carlo Biffi, Jinning Duan, and Daniel Rueckert. Data efficient unsupervised domain adaptation for cross-modality image segmentation. In *International Conference on Medical Image Computing and Computer-Assisted Intervention*, 2019. 3
- [10] Katherine Crowson, Stella Biderman, Daniel Kornis, Dashiell Stander, Eric Hallahan, Louis Castricato, and Edward Raff. Vqgan-clip: Open domain image generation and editing with natural language guidance. In *European Conference on Computer Vision*, pages 88–105. Springer, 2022. 5
- [11] Zolnamar Dorjsembe, Hsing-Kuo Pao, Sodontavilan Odonchimed, and Furen Xiao. Conditional diffusion models for semantic 3d medical image synthesis. *arXiv preprint arXiv:2305.18453*, 2023. 3
- [12] Alexey Dosovitskiy, Lucas Beyer, Alexander Kolesnikov, Dirk Weissenborn, Xiaohua Zhai, Thomas Unterthiner, Mostafa Dehghani, Matthias Minderer, Georg Heigold, Sylvain Gelly, Jakob Uszkoreit, and Neil Houlsby. An image is worth 16x16 words: Transformers for image recognition at scale, 2021. 8, 3
- [13] Richard O Duda and Peter E Hart. Use of the hough transformation to detect lines and curves in pictures. *Communications of the ACM*, 15(1):11–15, 1972. 4
- [14] Boni E Elewski. Clinical diagnosis of common scalp disorders. In *Journal of Investigative Dermatology Symposium Proceedings*, pages 190–193. Elsevier, 2005. 1
- [15] Jerome H Friedman. Greedy function approximation: a gradient boosting machine. *Annals of statistics*, pages 1189–1232, 2001. 8
- [16] Kaiming He, Xiangyu Zhang, Shaoqing Ren, and Jian Sun. Deep residual learning for image recognition. In *Proceedings of the IEEE conference on computer vision and pattern recognition*, pages 770–778, 2016. 3
- [17] Sheng He, Rina Bao, Jingpeng Li, Patricia Ellen Grant, and Yangming Ou. Accuracy of segment-anything model (sam) in medical image segmentation tasks. *ArXiv*, abs/2304.09324, 2023. 3
- [18] Dan Hendrycks, Norman Mu, Ekin D Cubuk, Barret Zoph, Justin Gilmer, and Balaji Lakshminarayanan. Augmix: A simple data processing method to improve robustness and uncertainty. *arXiv preprint arXiv:1912.02781*, 2019. 7, 8, 2
- [19] Martin Heusel, Hubert Ramsauer, Thomas Unterthiner, Bernhard Nessler, and Sepp Hochreiter. Gans trained by a two time-scale update rule converge to a local nash equilibrium. *Advances in neural information processing systems*, 30, 2017. 6
- [20] Jonathan Ho, Ajay Jain, and Pieter Abbeel. Denoising diffusion probabilistic models. *Advances in neural information processing systems*, 33:6840–6851, 2020. 3, 5
- [21] Gao Huang, Zhuang Liu, Laurens Van Der Maaten, and Kilian Q Weinberger. Densely connected convolutional networks. In *Proceedings of the IEEE conference on computer vision and pattern recognition*, pages 4700–4708, 2017. 7, 8, 2
- [22] Boah Kim, Yujin Oh, and Jong-Chul Ye. Diffusion adversarial representation learning for self-supervised vessel segmentation. *ArXiv*, abs/2209.14566, 2022. 3
- [23] Hyungjoon Kim, Woogeol Kim, Jeheok Rew, Seungmin Rho, Jisoo Park, and Eenjun Hwang. Evaluation of hair and scalp condition based on microscopy image analysis. In *2017 International conference on platform technology and service (PlatCon)*, pages 1–4. IEEE, 2017. 2, 6, 8, 1
- [24] Jong-Hwan Kim, Segi Kwon, Jirui Fu, and Joon-Hyuk Park. Hair follicle classification and hair loss severity estimation using mask r-cnn. *Journal of Imaging*, 8(10):283, 2022. 1, 2
- [25] Minjeong Kim, Yujung Gil, Yuyeon Kim, and Jihie Kim. Deep-learning-based scalp image analysis using limited data. *Electronics*, 12(6):1380, 2023. 2
- [26] Alexander Kirillov, Eric Mintun, Nikhila Ravi, Hanzi Mao, Chloe Rolland, Laura Gustafson, Tete Xiao, Spencer Whitehead, Alexander C Berg, Wan-Yen Lo, et al. Segment anything. *arXiv preprint arXiv:2304.02643*, 2023. 2, 3, 6, 1
- [27] Gihyun Kwon and Jong Chul Ye. Diffusion-based image translation using disentangled style and content representation. In *The Eleventh International Conference on Learning Representations*, 2022. 5, 6, 7, 8, 2
- [28] Gihyun Kwon and Jong Chul Ye. Improving diffusion-based image translation using asymmetric gradient guidance. *arXiv preprint arXiv:2306.04396*, 2023. 6, 7, 8, 2

- [29] Yanyu Li, Geng Yuan, Yang Wen, Ju Hu, Georgios Evangelidis, Sergey Tulyakov, Yanzhi Wang, and Jian Ren. Efficientformer: Vision transformers at mobilenet speed. *Advances in Neural Information Processing Systems*, 35: 12934–12949, 2022. 3
- [30] Yanyu Li, Ju Hu, Yang Wen, Georgios Evangelidis, Kamyar Salahi, Yanzhi Wang, Sergey Tulyakov, and Jian Ren. Rethinking vision transformers for mobilenet size and speed. In *Proceedings of the IEEE/CVF International Conference on Computer Vision*, pages 16889–16900, 2023. 7, 8, 2
- [31] Ilya Loshchilov and Frank Hutter. Sgdr: Stochastic gradient descent with warm restarts. *arXiv preprint arXiv:1608.03983*, 2016. 2
- [32] Ilya Loshchilov and Frank Hutter. Decoupled weight decay regularization. *arXiv preprint arXiv:1711.05101*, 2017. 2
- [33] Alexander Quinn Nichol and Prafulla Dhariwal. Improved denoising diffusion probabilistic models. In *International Conference on Machine Learning*, pages 8162–8171. PMLR, 2021. 5
- [34] Nobuyuki Otsu. A threshold selection method from gray-level histograms. *IEEE transactions on systems, man, and cybernetics*, 9(1):62–66, 1979. 8, 1
- [35] Suresh Panjwani. Early diagnosis and treatment of discoid lupus erythematosus. *The Journal of the American Board of Family Medicine*, 22(2):206–213, 2009. 1
- [36] Nadia Peyravian, Sapna Deo, Sylvia Daunert, and Joaquin J Jimenez. The inflammatory aspect of male and female pattern hair loss. *Journal of inflammation research*, pages 879–881, 2020. 1
- [37] C Herbert Pratt, Lloyd E King, Andrew G Messenger, Angela M Christiano, and John P Sundberg. Alopecia areata. *Nature reviews Disease primers*, 3(1):1–17, 2017. 1
- [38] Ji Qi and Luis A Garza. An overview of alopecias. *Cold Spring Harbor perspectives in medicine*, 4(3), 2014. 4
- [39] Xuebin Qin, Zichen Zhang, Chenyang Huang, Masood Dehghan, Osmar R Zaiane, and Martin Jagersand. U2-net: Going deeper with nested u-structure for salient object detection. *Pattern recognition*, 106:107404, 2020. 3, 1
- [40] Robin Rombach, Andreas Blattmann, Dominik Lorenz, Patrick Esser, and Björn Ommer. High-resolution image synthesis with latent diffusion models. In *Proceedings of the IEEE/CVF conference on computer vision and pattern recognition*, pages 10684–10695, 2022. 3
- [41] Jarek P Sacha, Tamara L Caterino, Brian K Fisher, Gregory J Carr, R Scott Youngquist, Brian M D’Alessandro, Anthony Melione, Douglas Canfield, Wilma F Bergfeld, Melissa P Piliang, et al. Development and qualification of a machine learning algorithm for automated hair counting. *International Journal of Cosmetic Science*, 43:S34–S41, 2021. 2
- [42] Thais H Sakuma and Howard I Maibach. Oily skin: an overview. *Skin pharmacology and physiology*, 25(5):227–235, 2012. 1
- [43] Sunyong Seo and Jinho Park. Trichoscopy of alopecia areata: hair loss feature extraction and computation using grid line selection and eigenvalue. *Computational and Mathematical Methods in Medicine*, 2020, 2020. 1, 2
- [44] Huang-Chia Shih. An unsupervised hair segmentation and counting system in microscopy images. *IEEE Sensors Journal*, 15(6):3565–3572, 2014. 2, 6, 1
- [45] Huang-Chia Shih and Bo-Syun Lin. Hair segmentation and counting algorithms in microscopy image. In *2015 IEEE International Conference on Consumer Electronics (ICCE)*, pages 612–613. IEEE, 2015. 4
- [46] Karyn Springer, Matthew Brown, and Daniel L Stulberg. Common hair loss disorders. *American family physician*, 68(1):93–102, 2003. 1
- [47] Brandon Trabucco, Kyle Doherty, Max Gurinas, and Ruslan Salakhutdinov. Effective data augmentation with diffusion models. *arXiv preprint arXiv:2302.07944*, 2023. 3
- [48] Sara Vestergren and Navid Zandpour. Automatic image segmentation for hair masking: two methods, 2019. 2
- [49] Anna Wałkiel-Burnat, Joanna Czuwara, Leszek Blicharz, Małgorzata Olszewska, and Lidia Rudnicka. Differential diagnosis of red scalp. the importance of trichoscopy. *Clinical and Experimental Dermatology*, page 11ad366, 2023. 1
- [50] Ross Wightman. Pytorch image models. <https://github.com/rwightman/pytorch-image-models>, 2019. 2
- [51] Saining Xie, Ross Girshick, Piotr Dollár, Zhuowen Tu, and Kaiming He. Aggregated residual transformations for deep neural networks. In *Proceedings of the IEEE conference on computer vision and pattern recognition*, pages 1492–1500, 2017. 8, 3
- [52] Gongtao Yue, Chengcheng Ji, Yongsheng Yang, et al. Hair counting method based on image processing technology. *Journal of Artificial Intelligence Practice*, 4(1):23–29, 2021. 2, 6, 1
- [53] Sangdoon Yun, Dongyoon Han, Seong Joon Oh, Sanghyuk Chun, Junsuk Choe, and Youngjoon Yoo. Cutmix: Regularization strategy to train strong classifiers with localizable features. In *Proceedings of the IEEE/CVF international conference on computer vision*, pages 6023–6032, 2019. 2
- [54] Hongyi Zhang, Moustapha Cisse, Yann N Dauphin, and David Lopez-Paz. mixup: Beyond empirical risk minimization. *arXiv preprint arXiv:1710.09412*, 2017. 2
- [55] Richard Zhang, Phillip Isola, Alexei A Efros, Eli Shechtman, and Oliver Wang. The unreasonable effectiveness of deep features as a perceptual metric. In *Proceedings of the IEEE conference on computer vision and pattern recognition*, pages 586–595, 2018. 5, 6
- [56] T. Y. Zhang and C. Y. Suen. A fast parallel algorithm for thinning digital patterns. *Commun. ACM*, 27(3):236–239, 1984. 3
- [57] Zheyuan Zhang, Lanhong Yao, Bin Wang, Debesh Jha, Elif Keles, Alpaly Medetalibeyoglu, and Ulas Bagci. Emit-diff: Enhancing medical image segmentation via text-guided diffusion model. *arXiv preprint arXiv:2310.12868*, 2023. 3
- [58] Zhun Zhong, Liang Zheng, Guoliang Kang, Shaozi Li, and Yi Yang. Random erasing data augmentation. In *Proceedings of the AAAI conference on artificial intelligence*, pages 13001–13008, 2020. 3
- [59] Xueyan Zou, Jianwei Yang, Hao Zhang, Feng Li, Linjie Li, Jianfeng Gao, and Yong Jae Lee. Segment everything everywhere all at once. *ArXiv*, abs/2304.06718, 2023. 3

Scalp Diagnostic System With Label-Free Segmentation and Training-Free Image Translation

Supplementary Material

This supplementary material provides additional details and extended results that complement the main paper. Included in this supplementary material are the following sections:

- Section **A** delves into detailed explanations of various medical scalp diseases.
- Section **B** offers a comprehensive look at our experimental setup and provides supplementary information.
- Section **C** introduces pseudo training set for training the hair segmentation model.
- Section **D** presents further insights into our approach to scalp disease classification.
- Section **E** extends the discussion on the selection and analysis of features used in predicting the severity of alopecia.
- Section **F** shows additional qualitative results of DiffuseIT-M.

A. Detailed Overview of Scalp Diseases

The dataset from AI-Hub³ categorizes scalp images into three primary conditions: *dandruff*, *excess sebum*, and *erythema*.

Dandruff, also referred to as a milder manifestation of seborrheic dermatitis, is characterized by the non-inflammatory exfoliation of dead epidermal cells from the scalp. While it can induce mild itching, it generally does not precipitate erythema or the formation of scabs [4].

Hyperseborrhea, the excessive production of sebum, represents a common aesthetic concern, manifested through the secretion of excess oil from hypertrophic sebaceous glands. This condition results in a shiny, oily skin appearance. Although sebum plays a crucial role in maintaining skin hydration and its protective barrier, its excessive secretion can lead to various dermatological issues. One such issue is the formation of sebum plugs, which are small, yellowish, or pale bumps that appear on the skin [42].

Scalp erythema, also known as red scalp, is characterized by widespread redness across the scalp. It can arise from several conditions, including psoriasis, seborrheic dermatitis, contact dermatitis, diffuse lichen planopilaris, dermatomyositis, and scalp rosacea [49].

B. Implementation Details

Hair segmentation. For our heuristic-driven hair segmentation, we utilized the U²-Net [39] official source code to

³<https://aihub.or.kr>

train 3,000 pseudo image-label pairs. The training parameters included a batch size of 32, a constant learning rate of 0.001, 100 training epochs, and the Adam optimizer. The output from U²-Net was binarized to obtain \hat{M} , using a threshold of 0.5.

Since other previous studies, excluding SAM [26], do not have an official codebase, we implemented their approaches based on descriptions in their papers, using OpenCV. For instance, [44] used contrast stretching and binary thresholding to derive the hair mask. [52] applied morphological operations, while [23] used Otsu’s method [34] for hair mask acquisition. In evaluating SAM, the mask with the highest Intersection over Union (IoU) score was selected as the final prediction.

Image augmentation. For DiffuseIT-M, detailed in Section 3.3 of the main paper, we construct a loss function for image translation while preserving hair content. This function is defined as follows:

$$\ell_{total}(x; x_{src}, x_{trg}, M) = \lambda_1 \ell_{style} + \lambda_2 \ell_{content} + \lambda_3 \ell_{mask} + \lambda_4 \ell_{sem} + \lambda_5 \ell_{rng}. \quad (18)$$

To incorporate the semantic information of the target image, we establish the style loss function, ℓ_{style} . This function leverages the [CLS] token from the last layer of DINO-ViT [6]. Denoting the [CLS] tokens as \mathbf{c} , the style loss is expressed as:

$$\ell_{sty}(x_{trg}, \hat{x}_0(x_t)) = \|\mathbf{c}(x_{trg}) - \mathbf{c}(\hat{x})\|_2 + \lambda_{mse} \|x_{trg} - \hat{x}_0(x_t)\|_2, \quad (19)$$

where λ_{mse} is set to 3,000, and the weight for ℓ_{style} , λ_1 , is set to 2,000.

The content loss, $\ell_{content}$, is designed to preserve the structure of source images. Let $k_i^l(x)$ represent the i -th key extracted from the l -th multi-head self-attention layer in DINO-ViT for image x . The content loss is then defined as:

$$\ell_{content} = \lambda_{sim} \ell_{sim}(x_{src}, \hat{x}_0(x_t)) + \lambda_{con} \ell_{con}(x_{src}, \hat{x}_0(x_t)), \quad (20)$$

where the similarity loss, ℓ_{sim} , and the content loss, ℓ_{con} , are

$$\ell_{sim}(x_{src}, \hat{x}_0(x_t)) = \|\cos_{ij}(x_{src}), \cos_{ij}(\hat{x}_0(x_t))\|_2, \quad (21)$$

$$\ell_{con}(x_{src}, \hat{x}_0(x_t)) = \text{infoNCE}(k_i^l(x_{src}), k_i^l(\hat{x}_0(x_t))), \quad (22)$$

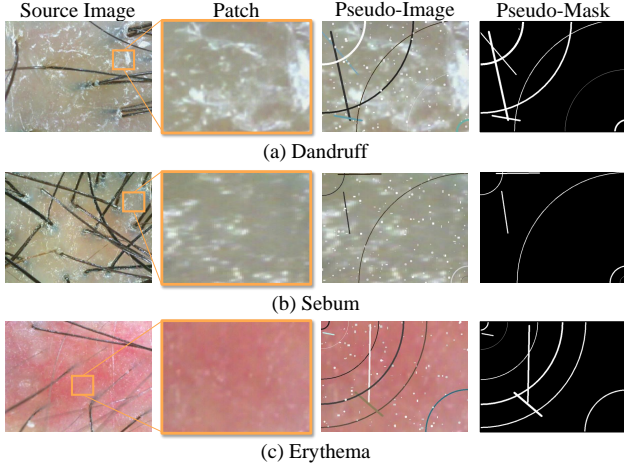


Figure 11. Examples of pseudo images and their corresponding masks for hair segmentation.

with $\cos_{ij}(x)$ representing the cosine distance between $k_i^l(x)$ and $k_j^l(x)$. The weights λ_{sim} and λ_{con} are set to 1,000 and 200, respectively. Additionally, weights λ_3 , λ_4 , and λ_5 are set to 1,000, 100, and 200, respectively. During our experiment, the model is configured to generate images with a resolution of 256×256 pixels, utilizing a denoising step of 1,000.

For implementation previous studies, we have performed the official source code of both DiffuseIT [27] and AGG [28], conducting experiments with the provided hyperparameters.

For the implementation of previous studies, we used the official source code of DiffuseIT [27] and AGG [28], conducting experiments with their provided hyperparameters. Non-generative image augmentations were performed using AugMix [18] through the torchvision library and Gaussian noise augmentation via the PyTorch library.

Scalp disease and severity diagnosis. For the classification task, we fine-tuned two models: DenseNet169 [21] (CNN-based) and EfficientFormerV2 [30] (Transformer-based), using pre-trained weights from the timm library [50]. Fine-tuning involved a batch size of 128, a learning rate of 0.0001 with a CosineAnnealingWarmRestarts scheduler [31], 50 training epochs, and the AdamW optimizer [32].

Alopecia severity prediction. To predict the severity of alopecia, we focused on extracting hair-related features, specifically hair thickness and count. For this, we employed the OpenCV library, utilizing Non-Maximum Suppression (NMS), Morphology operation, and Hough transformation techniques. These features were then used to train a prediction model with the GradientBoosting Classifier, a component of the Scikit-learn library [5]. The model’s training parameters were set as follows: a cross-entropy loss func-

Algorithm 2 Calculation of sampling ratios for each disease

Input: *severities*: A collection of records for each severity. Assume that each element of *severities* is classified as 0 (*good*), 1 (*mild*), 2 (*moderate*), and 3 (*severe*).

Output: *ratios*: Sampling ratio among four severity levels.

```

1:  $\epsilon \leftarrow 1 \times 10^{-9}$ 
2:  $sevCounts \leftarrow \{\}$ 
3: for each sevLevel in [0, 1, 2, 3] do
4:    $sevCounts[sevLevel] \leftarrow 0$ 
5: end for
6: for each severity in severities do
7:    $sevCounts[severity] \leftarrow sevCounts[severity] + 1$ 
8: end for
9:  $invCounts \leftarrow \{\}$ 
10: for each sevLevel in [0, 1, 2, 3] do
11:    $invCounts[sevLevel] \leftarrow 1/(sevCounts[sevLevel] + \epsilon)$ 
12: end for
13:  $normFactor \leftarrow \sum_{sevLevel=0}^3 invCounts[sevLevel]$ 
14:  $ratios \leftarrow []$ 
15: for each sevLevel in [0, 1, 2, 3] do
16:    $ratio \leftarrow invCounts[sevLevel]/normFactor$ 
17:    $ratios[sevLevel] \leftarrow ratio$ 
18: end for
19: return ratios

```

tion, a learning rate of 0.01, a maximum depth of 5, 3,000 estimators, and a subsample ratio of 1. All other parameters remained at their default settings in Scikit-learn.

In comparison, for the image-based models, we trained DenseNet169 and EfficientFormerV2 using similar hyperparameters as those used for scalp disease classification. The key differences were the employment of the cross-entropy loss function and the use of the Adam optimizer for these models.

C. Pseudo Image and Mask Visualization

To create a diverse pseudo training set, we extracted scalp patch images from areas without hair in nine different scalp images. Each image represented a unique disease at a specific severity level. As illustrated in Figure 11, we introduced a variety of hair types by inserting straight and curved lines in blue, brown, black, and white colors, each with differing thicknesses. To simulate common scalp noise, such as dandruff, white circular elements were added to the pseudo images. Our codebase contains further details on this process.

D. Scalp Disease and Severity Classification

This section outlines our data augmentation approach for classifying scalp diseases and their severities and presents additional experimental results.

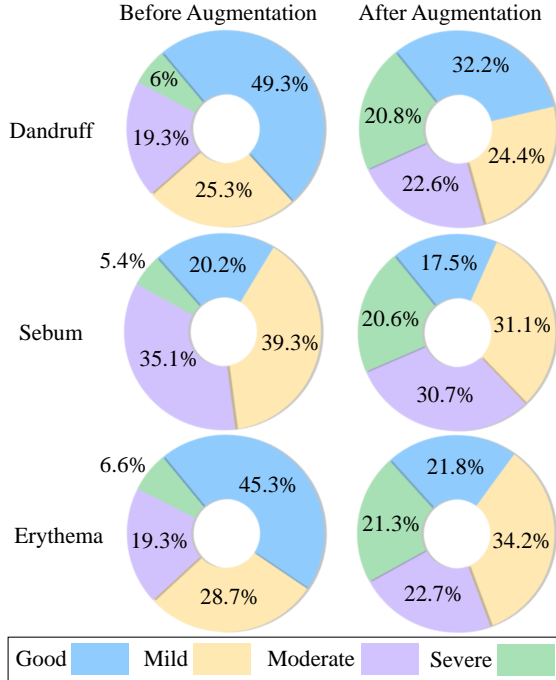


Figure 12. Data distribution of AI-Hub scalp dataset before and after the application of augmentation techniques.

D.1. Data Augmentation Strategy

Addressing the issue of data imbalance in the dataset, we implemented a strategy to translate randomly selected images into classes with fewer samples. We used random selection for the source images and weighted sampling for target images, where the likelihood of choosing an image was inversely proportional to the number of samples in its severity class. This method favored the selection of underrepresented classes. The algorithm to calculate these sampling weights is detailed in Algorithm 2.

Figure 12 displays the data distribution before and after this augmentation. The post-augmentation distribution shows a more balanced representation across various classes, especially a rise in the *severe* category and a reduction in the *good* category. This balanced dataset played a crucial role in enhancing our model’s performance by providing an even distribution of the training samples. The same augmentation strategy was applied across all diffusion-based methods.

D.2. Impact of Backbone Model

We assessed the performance of scalp disease classification using different pretrained backbone models. Our evaluation metric was the F1 macro score, which we also used to compare our results with existing augmentation methods, including those utilizing DiffuseIT and AGG. The experiments involved two CNN-based models (ResNet [16]

Table 8. Quantitative comparison of classification performance across different backbone models. “Baseline” refers to performance without any augmentation methods, while results following the “+” symbol indicate the use of various augmentation methods. Values in the table represent the macro-F1 scores.

Method	CNN		Transformer	
	ResNet	ResNeXt	EfficientFormer	ViT
Baseline	0.5709	0.6186	0.5300	0.4934
+ Gaussian Noise	0.4304	0.5663	0.5742	0.4306
+ AugMix	0.4186	0.5247	0.5348	0.4747
+ DiffuseIT	0.6064	0.6107	0.6120	0.5767
+ AGG	0.5978	0.6251	0.6104	0.5771
+ Ours	0.6128	0.6292	0.6170	0.5861

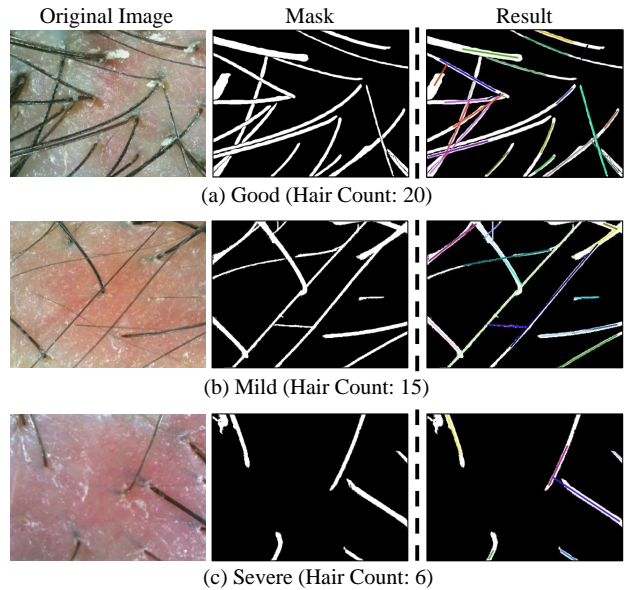


Figure 13. Qualitative results of hair count estimation. The displayed lines on the masks represent the line segments identified through the Hough Transformation.

and ResNeXt [51]) and two Transformer-based models (ViT [12] and EfficientFormer [29]), all maintaining consistent hyperparameters as described in Section B.

As presented in Table 8, our approach achieved superior classification performance across all backbone models. Moreover, models augmented using generative methods consistently outperformed those using baseline augmentation, validating the effectiveness of our proposed data augmentation strategy.

E. Alopecia Severity Prediction

E.1. Feature Selection for Severity Estimation

We identified key features for alopecia severity prediction, focusing on hair thickness and count. For thickness, we

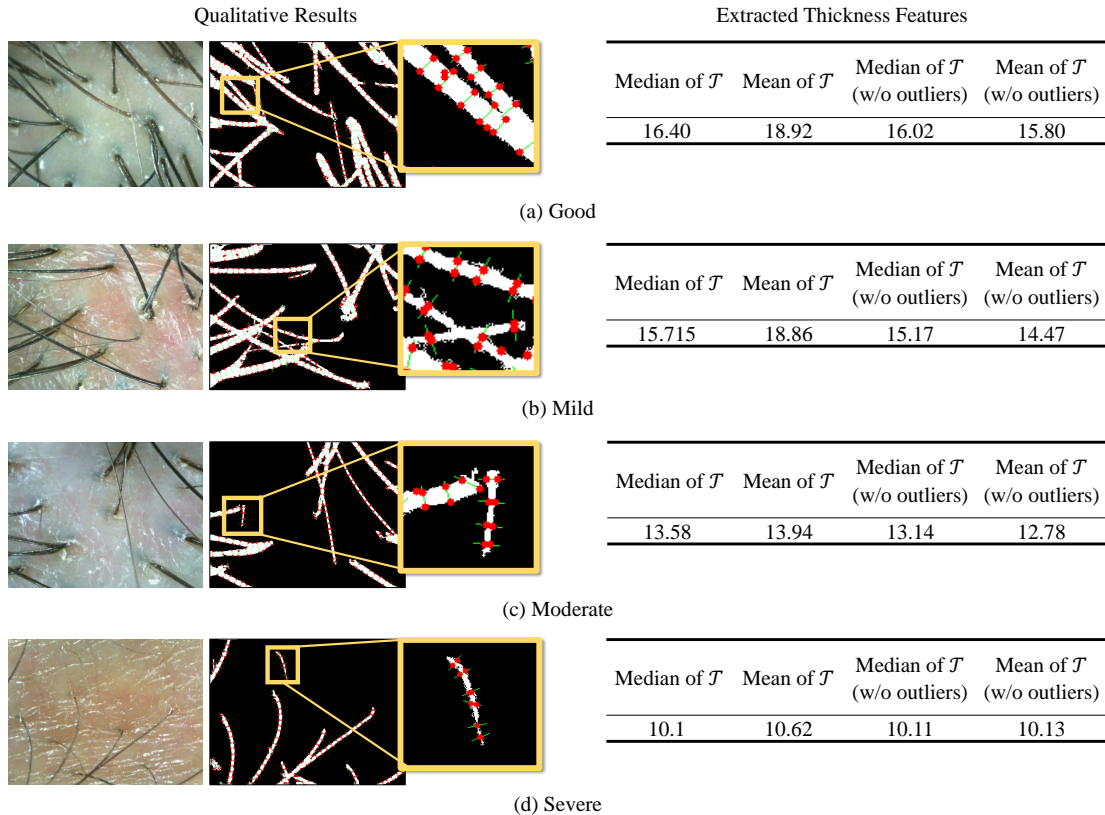


Figure 14. Qualitative results and estimated features of hair thickness estimation. The red dots on the image indicate the intersection points of hair strands and perpendicular line of hair direction, while the green lines represents the perpendicular lines. Each caption represents severity of alopecia.

analyzed the length of list B and computed the mean and median values of \mathcal{T} , excluding outliers identified using the interquartile range (IQR). We also considered the mean and median of the entire \mathcal{T} . Additionally, the number of line segments detected by the hair count estimator was used as a supplementary feature.

E.2. Visualization of Severity Features

Our method estimates hair thickness using mask images. Figure 13 showcases the qualitative results of our multi-scale Hough transform, which effectively distinguishes individual hairlines in the mask images. In Figure 14, we demonstrate thickness estimation across various scenarios for four alopecia severity classes: *good*, *mild*, *moderate*, and *severe*. Our segmentation successfully identified different hair thicknesses and distinguished hair from severe scalp conditions like dandruff or erythema. Notably, as alopecia severity increased, the feature values related to hair thickness decreased, validating the effectiveness of our approach.

F. Qualitative Results of DiffuseIT-M

Figure 15 presents qualitative results of our model’s ability to translate images across multiple labels while maintaining hair information. The results indicate that our model successfully translates various disease features from target images, effectively preserving hair representation.

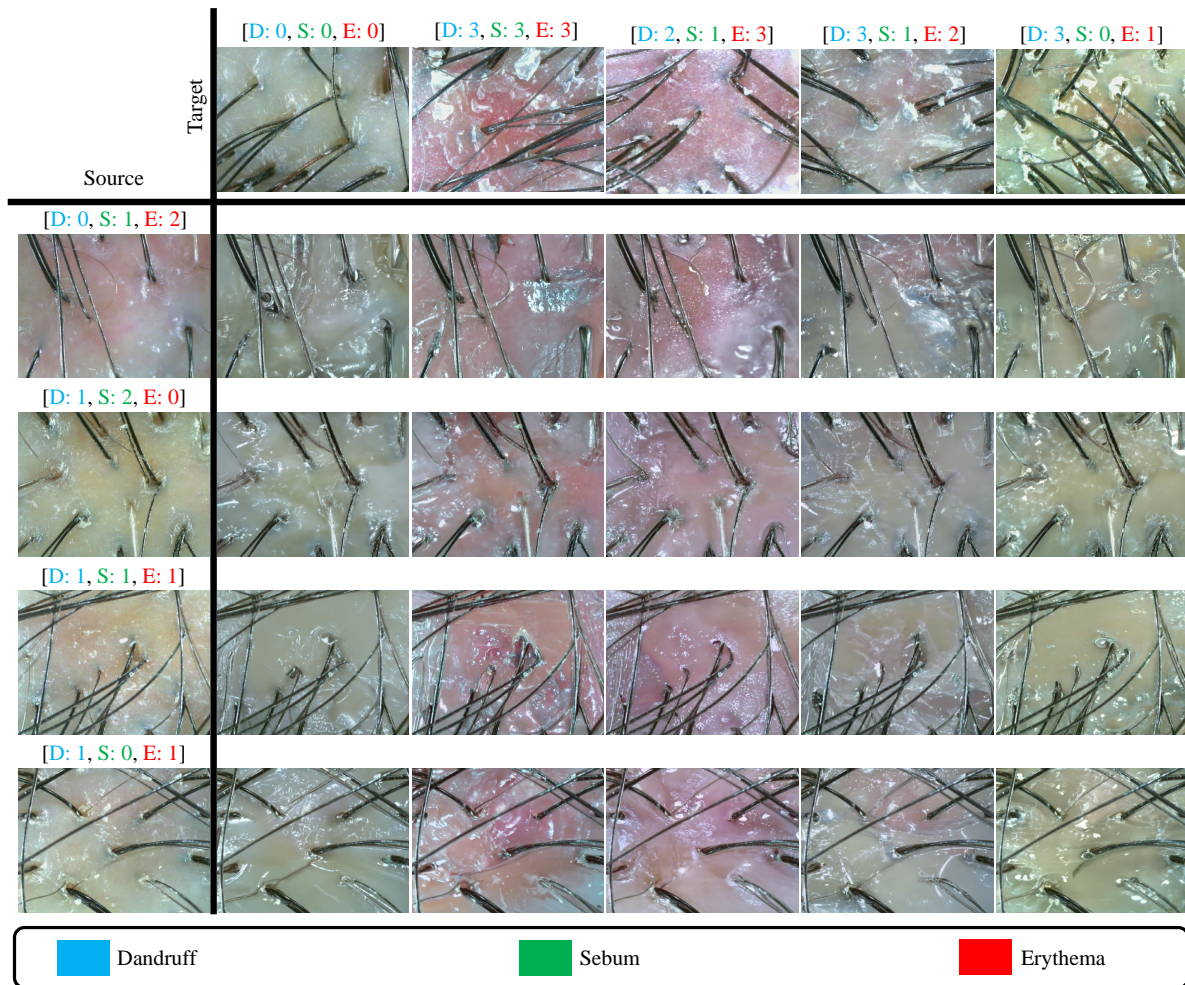


Figure 15. Qualitative results of DiffuseIT-M. This figure illustrates the results for various scalp disease conditions, with severity levels indicated as 0 (*good*), 1 (*mild*), 2 (*moderate*), and 3 (*severe*). Scalp diseases are color-coded for clarity: **blue** represents dandruff, **green** signifies excess sebum, and **red** denotes erythema.